Astroparticle Physics 148 (2023) 102820

Contents lists available at ScienceDirect

Astroparticle Physics

journal homepage: www.elsevier.com/locate/astropartphys

Criticality and phase transition of Kerr–anti-de Sitter black hole with quintessence and cloud of strings

Qanitah Ama-Tul-Mughani [a], Rabia Saleem [b,*], Wardat Us Salam [c], Sobia Sadiq [c]

[a] Department of Physics and Mathematics, Superior University Lahore, Gold Campus, Pakistan
[b] Department of Mathematics, COMSATS University Islamabad, Lahore Campus, Pakistan
[c] Department of Mathematics, Division of Science and Technology, University of Education, Lahore, Pakistan

ARTICLE INFO

Keywords:
Black hole thermodynamics
Maxwell equal-area law
Phase transition
Thermal fluctuations

ABSTRACT

In this paper, a thermodynamical study of the Kerr–anti-de Sitter (KAdS) black hole (BH) encircled by quintessence matter and the cloud of strings is presented. We check the effects of the cloud parameter on the thermodynamical variables including Hawking temperature, entropy, Helmholtz free energy (HFE), Gibbs free energy (GFE), and specific heat capacity. These thermodynamic variables hold the Smarr–Gibbs–Dehum (SGD) relation in the appearance of quintessence and the cloud of the string parameter. Then we calculate the critical expressions of the developed variables in two different ways that are "Van-der-Waals (vdW)-type equation of state" (EoS) and the "Maxwell equal-area law" (MEAL). The latter technique is found to be more reasonable to examine the criticality of the complex BHs. Using MEAL, we plot the phase diagram in a temperature–entropy plane and obtain an isobar, which represents the co-existence region of liquid–gas phases. It is concluded that the uncharged BHs exhibit the same phase transition (PT) to vdW fluid as the temperature drops down its critical value. Also, we discuss the influence of thermal fluctuations (TF) on the stability of KAdS BH.

1. Introduction

A notion of the cloud of strings is presented as a configuration of one-dimensional objects from the string theory, which can be effective on gravitational fields such as BHs. The strings are believed to be fundamental objects in the universe which motivates researchers to study their impact on various gravitational fields. It is well-known that strings cloud influences the structure of the event horizon. Letelier [1] introduced a criterion to derive the exact solutions of the Einstein field equations (EFEs) for a BH surrounded by the strings cloud. In his work, various studies were listed in which formalism has been implemented on the geometries with the plane, spherical and cylindrical symmetries. Among them, the spherical symmetry is of main concern, as it is the generalization of the Schwarzschild BH (SBH) solution. Alternatively, it is a modified version of the SBH solution, where the cloud of strings is an extra gravitational source. In this extended solution, if a mass of the BH is considered zero, then only the strings cloud is left, for which there will be no horizon, but a singularity (naked) exists at $r = 0$. Going back to the combined origins, BH and strings cloud, it has resulted that the existence of the strings cloud furnishes with an effect of "global origin" is related to a solid deficit angle, depending on the cloud parameter, similarly to what takes place in the geometry of a global monopole [2]. So, the presence of global origin can give conceivable astrophysical outcomes that advocate the importance of the strings cloud in this phenomenon.

Bernard [3] discussed the presence of stationary massive charged scalar clouds around Kerr–Sen BHs. He also studied stationary scalar clouds within the context of static electrically charged BHs in low-energy limit of heterotic string theory, i.e., the Gibbons–Maeda–Garfinkle–Horowitz–Strominger BHs. Tokgöz and Sakalli [4] investigated the dynamics of charged massive scalar field propagating in an extremal linear dilaton BH. They found the existence of clouds enclosing the BHs and computed effective heights of clouds above the center of BH. Al-Badawi et al. [5] examined the effect of quintessence parameter on regular Bardeen BH via physical behaviors of the effective potentials. They also studied the greybody factors of bosons and fermions from the Bardeen BH surrounded by quintessence. The same authors in [6] solved the Dirac equation for $z = 0$ (z is a dynamical exponent) Lifshitz BH spacetime and employed Maggiore's method to obtain the entropy/area spectra of the considered spacetime, which are shown to be equidistant. Sadeghi et al. [7] discussed the constant corrections to general relativity and found a relationship between entropy and extremal-bound for charged-rotating-AdS BH and extended these

* Corresponding author.
E-mail addresses: qanitah@superior.edu.pk (Q. Ama-Tul-Mughani), rabiasaleem@cuilahore.edu.pk (R. Saleem), wardat.salam@ue.edu.pk (W.U. Salam), sobia.sadiq@ue.edu.pk (S. Sadiq).

https://doi.org/10.1016/j.astropartphys.2023.102820
Received 24 August 2022; Received in revised form 17 October 2022; Accepted 31 January 2023
Available online 14 February 2023

calculations for BH are surrounded by the quintessence and cloud of strings. They also developed a relation between extremal mass of BH and the parameter of the cloud string. They noted that the constant correction is inversely related to the entropy of BH, which leads to a decrease in the mass-to-charge ratio which fully confirms the BH's weak gravity conjecture. Al-Badawi [8] investigated the greybody factor for the Schwarzschild BH immersed in quintessence and associated with a cloud of strings. He found that the greybody factor is strongly influenced by the shape of potential. Sakalli and Kanzi [9] discussed a pedagogical introduction as well as some recent developments in BHs, greybody factors, and quasinormal modes. They studied some particular analytical/approximation techniques for the computations of greybody factors and quasinormal modes.

According to recent astronomical observations, it has become an ultimate fact that our universe is passing through an accelerating expanding stage, which is one of the most astonishing discoveries in the field of observational cosmology [10]. On a large scale structure, this fact emphasizes the presence of an energy component that acts opposite to gravitational force and must possess negative pressure. This type of anti-gravitational force with constant energy density is called quintessence or quintessence dark energy (QDE) [11], in which pressure can be written in terms of energy density with an EoS $P = w\rho$. Here, the EoS parameter w must lies in the interval $(-1, -\frac{1}{3})$ to achieve the required cosmic acceleration. This permeates the cosmos and finally covered a BH, and gives worthy results in astrophysics. Therefore, it is crucial to find the analytic solution of the EFEs for BHs encircling by QDE as worked out by Kiselev [11]. This idea is extensively being studied in literature like Kiselev solution [11] was generalized by Chen et al. [12] to d-dimensional space–time considering that QDE did not lie just on the brane but also in the bulk.

Thermodynamical analysis of BH is one of the active and important research topics in gravitational physics and general relativity. From the 1970's up to now, the studies of Bekenstein [13,14] and Hawking [15–17] provide a deep understanding of quantum gravity. Lately, the studies of BHs PT in asymptotically AdS spacetime have rising interest, as these PTs are connected to the holographic superconductivity of AdS/CFT correspondence scenario [18]. Recent publications have manifested that the RN–AdS BH has equivalent critical thermodynamic properties to a vdW system. The authors in [19] proposed a connection between cosmological constant (Λ) and pressure for charged spherically symmetric AdS BH in higher-dimensional geometry. Their results showed that BH and the vdW liquid–gas system are analogous, keeping the foundations of BH thermodynamics in extended phase space (EPS). Whereas, SBH has no similar PT to the vdW system, which is done by Zhang et al. [20]. It is a proven result that the isothermal trajectories in the vdW fluid exhibit the same trend as the experimental outcomes when the temperature surpasses its critical value. However, an oscillating region is obtained for the temperature below the critical temperature, which violates the stable equilibrium condition. Later, some characteristics of AdS BH with charge were analyzed including pressure–volume or temperature–entropy criticality, critical values ratio, PT of the first order, etc [21–23].

Gunasekaran and his collaborators [24] found the critical expressions of thermodynamic variables for charged and rotating AdS BH in EPS and represented its equivalence with vdW liquid–gas system. Cheng et al. [25] examined the criticality of Kerr–Newman–AdS (KNAdS) BH in EPS and found the critical points numerically for the vdW-type PT. Sadeghi with Kubeka [26] investigated the $P-V$ criticality of modified Bañados–Teitelboim–Zanelli (BTZ) BH satisfying the liquid–gas PT EoS. Graça et al. [27] studied the BH thermodynamics in the presence of cloud of strings in the vicinity of general relativity as well as $f(R)$ theory of gravity. The authors in [28] examined thermal characteristics and PT for rotating Hayward–dS BHs, and showed that regular BHs have low temperature as compared to the singular BHs. Singh and Siwach [29] analyzed the thermal and critical nature of Bardeen–AdS BH, and resulted that the derived solutions belong to the class of vdW fluid. Wei and Liu [30] studied the PT and micro-structures of charged AdS BH in the Gauss–Bonnet gravity.

It has been proved that the charged AdS BH surrounded by QDE represented a BH PT in a similar manner to liquid–gas PT of the vdW system. Li [31] studied the impact of DE on the critical nature of $P-V$ diagram for RN–AdS BH and proved that QDE does not affect the occurrence of small or large BH PT. The effects of DE on the criticality of charged rotating BH for different values of w has also been studied by Jafarzade and Sadeghi [32]. Utilizing MEAL, Guo [33] determined the PT of charged AdS BHs surrounded by QDE, and resulted that such BHs showed the same PT as that of the vdW system. Sharif and Ama-Tul-Mughani [34] discussed the effects of quintessence parameter as well as EoS parameter on the thermodynamics of BH (having charge as well as rotating attributes). They observed that the temperature of BH decreases for the larger values of quintessence parameter. The same authors [35] studied the PT of quintessential Kerr–Sen–AdS BHs and found that below the critical pressure, BHs observe similar PT as that of liquid–gas vdW fluid. Recently, the thermodynamics of RN–AdS BH surrounded by a cloud of strings and QDE has been discussed via different thermodynamic variables [36]. Chabab and Iraoui [37] worked on an exact solution for charged AdS BHs surrounded by QDE and strings cloud in higher dimensional geometry.

The effects of TF on BH geometry have extensively been studied in literature [38]. Pourhassan with his collaborators [39] found logarithmic entropy corrections about the equilibrium point and checked the duality of vdW fluid. Haldar and Biswas [40] studied the thermodynamic properties of regular BHs taking statistical fluctuations and concluded that all thermodynamic variables exhibit decreasing trend versus correction parameter. Upadhyay [41] analyzed the influence of leading order corrections on the stability of charged rotating AdS BHs. They also found that thermodynamic potentials satisfy the first law of BH thermodynamics (FLBT). The influence of first order corrections on the PT of KN–AdS BH have been analyzed in [42]. Similarly, Zhang [43] examined the physical trend of thermodynamic potentials of RN–AdS and KN BHs taking first-order corrections. Sharif and Akhtar [44] discussed quasi-normal modes and TF of charged BH with Weyl corrections. Ama-Tul-Mughani and her collaborators [45] studied the impact of TF on the thermodynamics of various BH geometries.

We aim to analyze the combined effects of QDE and cloud of strings on the criticality and PT of rotating KAdS BH. We develop thermodynamical variables including Hawking temperature, pressure, free energy, angular velocity (AV), and SGD relation. Then we calculate the exact critical expression of all these quantities through two techniques and discuss the PT of the considered BH. The paper is assembled as follows. The next section elaborates the spacetime geometry and thermodynamical quantities. Then, the critical behavior of $P-V$ diagram for uncharged KN–AdS BH with QDE and strings cloud is discussed. In Section 3, MEAL is used in $T-S$ conjugate quantities to examine the constraints hold by PT. Section 4 furnishes the general equation of modified entropy and deals with stability of the model. The results are compiled in Section 5.

2. Kerr–AdS black hole with quintessence matter and cloud of strings

In "Boyer-Lindquist coordinates", the space–time of KAdS BH with QDE and strings cloud is written as

$$ds^2 = -\frac{\Delta_r}{\Omega}\left(dt - \frac{a\sin^2\theta}{\Xi}d\phi\right)^2 + \frac{\Omega}{\Delta_r}dr^2 + \frac{\Omega}{\check{P}}d\theta^2 + \frac{\check{P}\sin^2\theta}{\Omega}\left(adt - \frac{(r^2+a^2)}{\Xi}d\phi\right)^2, \quad (1)$$

where the involved terms are defined as under

$$\Delta_r = (1-b)r^2 + a^2 + (r^2+a^2)\left(\frac{r^2}{l^2}\right) - 2mr - \alpha r^{1-3w},$$

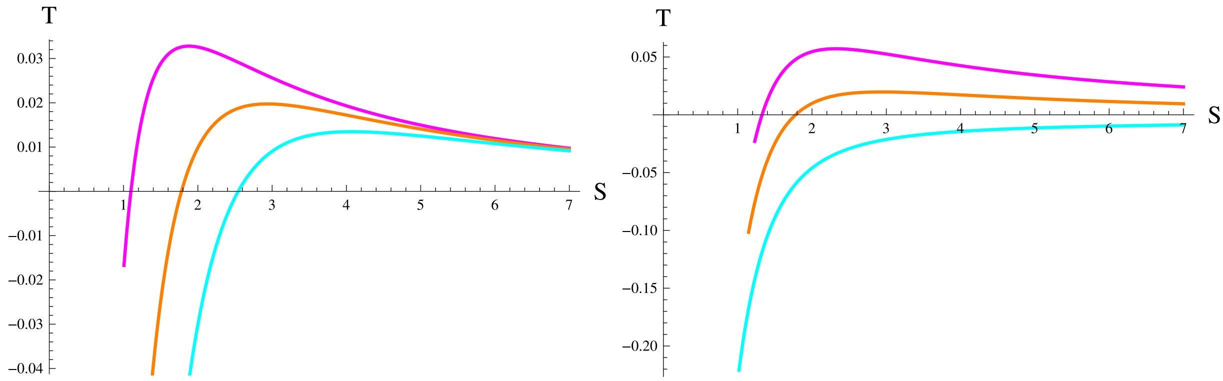

Fig. 1. Hawking temperature against entropy for $\alpha = 0.1$ and $w = -0.5$. Left plot by fixing $b = 0.5$ and varying $a = 0.2$ (magenta), 0.3 (orange), 0.4 (cyan). Right plot by fixing $a = 0.3$ and varying $b = 0.1$ (magenta), 0.5 (orange), 1 (cyan).

$$\Omega = r^2 + a^2\cos^2\theta, \quad \Xi = 1 - \frac{a^2}{l^2}, \quad \check{P} = 1 - \frac{a^2}{l^2}\cos^2\theta, \tag{2}$$

with rotation parameter a, mass of BH m, radius of AdS BH is determined by $l^2 = -\frac{3}{\Lambda}$, and quintessence parameter $\alpha \le \frac{2}{1-3w}8^w$, which determines the quintessence field intensity around the BH [46]. This inequality satisfies until the existence of horizon formed by QDE. The line-element given in (1) can be re-written in the following form

$$ds^2 = -\mathcal{A}(r,\theta)dt^2 + \frac{dr^2}{\mathcal{B}(r,\theta)} + \Sigma(r,\theta)d\theta^2 + D(r,\theta)d\phi^2 - 2E(r,\theta)dtd\phi, \tag{3}$$

with

$$\mathcal{A}(r,\theta) = \frac{\Delta_r - a^2\check{P}\sin^2\theta}{\Omega}, \quad \mathcal{B}(r,\theta) = \frac{\Delta_r}{\Omega}, \quad \Sigma(r,\theta) = \frac{\Omega}{\check{P}}, \tag{4}$$

$$D(r,\theta) = \frac{\check{P}\sin^2\theta\left(a^2+r^2\right)^2 - \Delta_r\left(a\sin^2\theta\right)^2}{\Xi^2\Omega}, \tag{5}$$

$$E(r,\theta) = \frac{a\check{P}\sin^2\theta\left(a^2+r^2\right) - \Delta_r a\sin^2\theta}{\Xi\Omega}. \tag{6}$$

The above line-element reduces to KAdS BH surrounded by QDE only for $b = 0$ whereas the KAdS BH solution is recovered for vanishing both $\alpha,\ b$.

2.1. Critical behavior and thermodynamical analysis in EPS

Here, we will analyze thermal characteristics and pressure–volume criticality of the KAdS BH covered by QDE and cloud of strings in an EPS. Under horizon constraint $\Delta(r_+) = 0$, the BH mass and entropy as a function of horizon radius r_+, respectively turn out to be

$$m = \frac{1}{2r_+}\left((1-b)r_+^2 + a^2 + \frac{r_+^2\left(a^2+r_+^2\right)}{l^2} - \alpha r_+^{1-3w}\right), \tag{7}$$

$$S = \frac{A}{4} = \frac{\pi\left(a^2+r_+^2\right)}{\Xi}, \quad \text{with} \quad A = \int_0^{2\pi}\int_0^{\pi}\sqrt{g_{\theta\theta}g_{\phi\phi}}|_{r=r_+}d\theta d\phi. \tag{8}$$

Entropy has an important role in thermodynamic evolution of a BH. It can be seen from its formula that the rotation parameter and horizon radius can affect entropy whereas it is independent of the cosmological constant, quintessence and strings cloud parameters. For the under consideration model, the Hawking temperature is computed as

$$T = \frac{\Delta_r'(r)}{4\pi(r^2+a^2)}|_{r=r_+} = \frac{\frac{r^2\left(a^2+3r^2\right)}{l^2} - a^2 + (1-b)r^2 + 3\alpha w r^{1-3w}}{4\pi r\left(a^2+r^2\right)}. \tag{9}$$

Figs. 1 and 2 represent the trend of Hawking temperature with respect to entropy. It can be seen from the graphs that temperature is sensitive for all the involved model parameters, and exhibits the same behavior. Fig. 1 shows that temperature decreases with the increase of rotation and strings cloud parameters $a,\ b$, then becomes constant after critical radius. The EoS parameter slightly affects the temperature of BH (left panel of Fig. 2), and the temperature drops down for increasing α (right panel of Fig. 2).

The corresponding AV is found to be

$$\omega_r = -\frac{g_{t\phi}}{g_{\phi\phi}} = \frac{a\check{P}\sin^2\theta\left(a^2+r^2\right) - \Delta_r a\sin^2\theta}{\check{P}\sin^2\theta\left(a^2+r^2\right)^2 - \Delta_r a^2\sin^4\theta}. \tag{10}$$

At the event horizon, the function of radius χ, becomes zero, which leads to following form of AV of the BH horizon

$$\omega_H = \frac{a\Xi}{\left(a^2+r_+^2\right)}. \tag{11}$$

It is already known that the AV of rotating BHs in AdS space is non-zero at infinity, i.e., $\omega_{r\to\infty} \neq 0$. This particular property distinguishes AdS space–time from the asymptotically flat space–time where $\omega_{r\to\infty}$ vanishes. For rotating BHs, the AV is given as

$$\omega = \omega_H - \omega_{r\to\infty} = \frac{a\left(l^2+r_+^2\right)}{l^2\left(a^2+r_+^2\right)}, \tag{12}$$

at $r \to \infty$, it becomes

$$\omega_{r\to\infty} = \frac{a}{l^2}. \tag{13}$$

Pressure along with its conjugate thermodynamic variable to the BH volume [24] are given by, respectively

$$P = \frac{3}{8\pi l^2}, \tag{14}$$

$$V = \frac{2\pi}{3l^2 r_+\left(1-\frac{a^2}{l^2}\right)^2}\left(a^2bl^2r_+^2 - \frac{2a^2bl^2r_+^2\left(l^2+r_+^2\right)}{a^2+r_+^2} - a^2\alpha l^2 r_+^{1-3w} + \left(a^2+r_+^2\right)\left(a^2l^2 - a^2r_+^2 + 2l^2r_+^2\right)\right). \tag{15}$$

The Mass (M) and angular momentum (J) (magnitude of rotational motion) are expressed as

$$M = \frac{m}{\Xi^2}, \quad J = \frac{ma}{\Xi^2}. \tag{16}$$

Taking product of Eqs. (8) and (9), we obtain

$$TS = \frac{\frac{8}{3}P\pi r_+^2a^2 + 8\pi P r_+^4 - a^2 + (1-b)r_+^2 + 3\alpha w r^{1-3w}}{4r_+\Xi}.$$

Using Eqs. (12), (14)–(16) (the expressions of w, P, V and J) alongwith the above equation, we rewrite $M = \frac{m}{\Xi^2}$ in terms of other thermodynamical variables as

$$M = 2(TS - PV + \omega J) + \alpha\Psi\left(-\frac{2a^2}{a^2+r_+^2} + 3w + 1\right), \tag{17}$$

which is known as the SGD relation. The involved physical quantity Ψ (conjugate to α) is given by $\Psi = -\frac{r_+^{-3w}}{2\Xi}$. The above relation also holds in the absence of quintessence [47] and a cloud of string parameter [34].

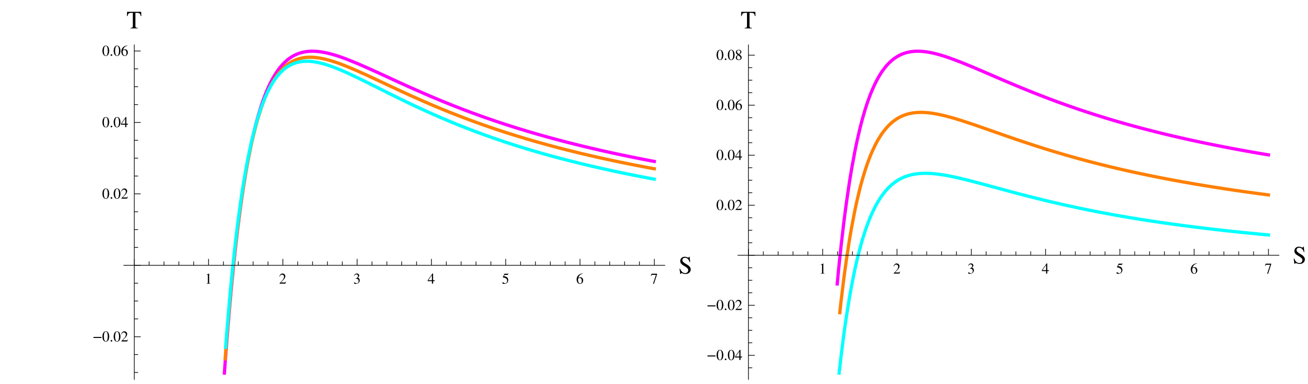

Fig. 2. Hawking temperature against entropy for $\alpha = 0.1$ and $a = 0.3$. Left plot by varying $w = -0.3$ (magenta), -0.4 (orange), -0.5 (cyan). Right plot by varying $\alpha = -0.1$ (magenta), 0.1 (orange), 0.3 (cyan).

It is checked that all the thermodynamic variables reduce to that of rotating KAdS BH for $\alpha,\ b = 0$ [24].

Now, we analyze the impact of QDE on the critical behavior of $P-V$ for KAdS BH. Using Eqs. (12) and (14), the Hawking temperature in terms of pressure can be written as

$$T = -\frac{a^2\left(\frac{3}{r_+} - 8\pi P r_+\right) + 3\left((b-1)r_+ - 8\pi P r_+^3 - 3\alpha w r_+^{-3w}\right)}{12\pi\left(a^2 + r_+^2\right)}. \tag{18}$$

Using Eqs. (2), (7) and (14), we rewrite the pressure in terms of temperature and angular momentum as

$$\begin{aligned} P =\ & \frac{T}{2r_+} - \frac{1}{8\pi r_+^2} + \frac{b}{8\pi r_+^2} - \frac{3\alpha w r_+^{-3w-3}}{8\pi} \\ & + \frac{3J^2\left(8\pi r_+^5 T + 3\alpha w r_+^{3-3w} + 4r_+^4 - 4br_+^4\right)}{8\pi r_+^6\left(2\pi r_+^3 T - \frac{3}{2}\alpha(w+1)r_+^{1-3w} + r_+^2 - br_+^2\right)^2} + O(J^4). \end{aligned} \tag{19}$$

Here the expansion of all quantities is restricted to $O(J^2)$ by neglecting higher order terms in J^2, so that complex computation can be avoided. We rewrite the rotation parameter as well as the cosmological constant in terms of angular momentum/pressure and using Eq. (15), we introduce a new variable v related to the specific volume of the vdW fluid as

$$v = 2\left(\frac{3V}{4\pi}\right)^{\frac{1}{3}} = 2r_+ + \frac{12J^2}{r_+}\left(\frac{-br_+^2 - \frac{3b}{4\pi P} + 8\pi P r^4 - \alpha r^{1-3w} + 3r_+^2}{\left(8\pi P r^4 - 3\alpha r^{1-3w} + 3r_+^2 - 3br_+^2\right)^2}\right), \tag{20}$$

which converts Eq. (19) to the following form

$$\begin{aligned} P =\ & \frac{b}{2\pi v^2} + \frac{48J^2}{\pi v^6} - \frac{1}{2\pi v^2} + \frac{T}{v} \\ & - \frac{3\alpha 8^w w v^{-3(w+1)}}{\pi} + \Bigg(48J^2\Bigg(-b^2v^4 + bv^4 \\ & - 3bv^4\left(1 - \frac{+\pi v^3 T + 3\alpha 8^w w(3w+1)v^{1-3w}}{bv^2 - v^2 + 2\pi v^3 T - 3\alpha 2^{3w+1} w v^{1-3w}}\right) + 3\pi b v^5 T - 7\alpha b 2^{3w} \\ & \times v^{3-3w} - 9\alpha b 2^{3w} w v^{3-3w} - 9\pi\alpha T 8^w w^2 v^{4-3w} - 5\pi\alpha T 2^{3w} v^{4-3w} - 3\pi\alpha T \\ & \times 2^{3w+1} w v^{4-3w} + 27\alpha^2 2^{6w} w^3 v^{2-6w} + 27\alpha^2 2^{6w} w^2 v^{2-6w} - 9\alpha 8^w w^2 v^{3-3w} \\ & - 9\alpha^2 2^{6w} v^{2-6w} - 9\alpha^2 2^{6w} w v^{2-6w} + 7\alpha 2^{3w} v^{3-3w} + 3\alpha 2^{3w} w v^{3-3w}\Bigg)\Bigg)\Bigg(\pi v^6 \\ & \times \left(v\left(-bv + v + \pi v^2 T - 3\alpha 8^w (w+1) v^{-3w}\right)\right)^2\Bigg)^{-1}. \end{aligned} \tag{21}$$

We use the following conditions are used to evaluate critical points

$$\frac{\partial P}{\partial v}|_{T=Tc} = \frac{\partial^2 P}{\partial v^2}|_{T=Tc} = 0. \tag{22}$$

Taking $\left(v_c^2 - bv_c^2 + \pi v_c^3 T - 3\alpha 8^w (w+1) v_c^{1-3w}\right)$ equal to unity and utilizing Eqs. (21) and (22), we can find the expression of critical temperature (T_c) given as under

$$\begin{aligned} T_c =\ & \Bigg(48J^2\Bigg(2b^2v_c^4\left(\frac{81\alpha 8^w w^2 v_c^{3w+3} + 27\alpha 8^w w v_c^{3w+3}}{\left(\left(3(b-1)v_c^2 + 2\right)v_c^{3w} + 3\alpha v_c 2^{3w+1}\right)^2} - 1\right) \\ & - \Bigg(bv_c^{3-3w}(-3\alpha 8^w v_c^{6w}(-3\left(21b^2 - 26b + 5\right)v_c^4 - 9w^2(3\left(3b^2 - 8b + 7\right)v_c^4 \\ & + 4(3b-4)v_c^2 + 4) - w\left(9\left(16b^2 - 33b + 19\right)v_c^4 + 6(32b-33)v_c^2 + 64\right) \\ & + (52 - 84b)v_c^2 + 27v_c^2 w^3\left(3(b-1)v_c^2 + 2\right) - 28) + 9\alpha^2 4^{3w+1} v_c^{3w+1} \\ & \times \left((21b-17)v_c^2 + 9w^2\left((3b-4)v_c^2 + 2\right) + w\left((48b-51)v_c^2 + 32\right) + 14\right) \\ & + 4\left(3(b-1)v_c^2 + 2\right)^2 v_c^{9w+1} + 27\alpha^3 v_c^2 2^{9w+2}\left(9w^2 + 16w + 7\right))\Bigg) \\ & \times \left(\left(\left(3(b-1)v_c^2 + 2\right)v_c^{3w} + 3\alpha v_c 2^{3w+1}\right)^2\right)^{-1} + 3v_c^{-6w}(-\alpha 8^w (9w^3 + 6w^2 \\ & - 10w - 7)v_c^{3w+3} + 3\alpha^2 v_c^2 2^{6w+1}\left(9w^4 + 15w^3 + 3w^2 - 5w - 2\right) + 2v_c^{6w})\Bigg) \\ & + v_c^{3-3w}\left((b-1)v_c^{3w+1} - 9\alpha 8^w w^2 - 9\alpha 8^w w\right)\Bigg)\Bigg(\pi v_c^7\Bigg(-\frac{144bJ^2 + 1}{v_c^2} \\ & + \frac{144bJ^2}{3(b-1)v_c^2 + 3\alpha 2^{3w+1} v_c^{1-3w} + 2} + 3\alpha J^2 2^{3w+4}\left(27w^3 + 36w^2 + 27w + 10\right) \\ & \times v_c^{-3(w+1)} + \frac{27\alpha b J^2 2^{3w+5}(3w-1)v_c^{3w+1} - 864(b-1)bJ^2 v_c^{6w+2}}{\left(\left(3(b-1)v_c^2 + 2\right)v_c^{3w} + 3\alpha v_c 2^{3w+1}\right)^2}\Bigg)\Bigg), \end{aligned} \tag{23}$$

here v_c is the critical value of specific volume, which can easily be obtained via Eqs. (21), (22) and (23). Substituting the expression of T_c in Eq. (21), we can find the critical pressure (P_c) which corresponds to the pressure at a critical point. For temperatures exceeding the critical value, matter cannot be liquified no matter the amount of pressure applied. So, the critical temperature is identified as the pressure applied to a substance to liquefy it at its critical temperature. Taking $w = -\frac{2}{3}$ and $b = 0$, the critical values of all the above mentioned quantities turn out to be

$$\begin{aligned} v_c &= 2\sqrt{3}\sqrt[4]{10}\sqrt{J}, \quad T_c = -\frac{\alpha}{2\pi} - \frac{12\alpha J^2}{\pi} + \frac{2^{3/4}}{5\sqrt{3}\sqrt[4]{5}\pi\sqrt{J}}, \\ P_c &= \frac{4\ 2^{3/4}\sqrt{3}\alpha J^{3/2}}{\sqrt[4]{5}\pi} - \frac{720\alpha^2 J^4}{\pi} - \frac{27\alpha^2 J^2}{\pi} + \frac{1}{36\sqrt{10}\pi J}. \end{aligned} \tag{24}$$

It is noted that the regular critical nature of Kerr BH can be obtained for $\alpha = 0$ [24]. For $w \neq -\frac{2}{3}$ in rotating BHs, the exact critical points are not calculated because of lengthy expressions of v_c. However, for other values of w, one can solve the expression of v_c numerically. Then P_c and T_c are obtained via Eqs. (20) and (23), respectively.

3. Development of Maxwell equal-area law in $T-S$ diagram

This section is devoted to examine the phase diagram of KAdS BH with QDE and strings cloud via MEAL in $T-S$ differential conjugate quantities. To this end, we have considered the parameters J, l, w and α as constants. T_0 ($T_0 \leq T_c$) lies on the vertical axis, depending upon the radius of the horizon whereas the horizontal axis of the two-phase co-existence space are S_2 and S_1, respectively. Thus, the MEAL has the following form

$$T_0(S_2 - S_1) = \int_{S_1}^{S_2} T\,dS,$$

for considered BH, it turn out to be

$$T_0(S_2 - S_1) = \int_{r_1}^{r_2} \Big(4\pi P r^2 + \frac{3}{2}\alpha w r^{-1-3w} + \frac{1-b}{2} + \frac{a^2}{r^4}\Big(-\frac{8}{3}\pi P r^4 - \frac{3}{2}\alpha w \times r^{1-3w} - (1-b)r^2\Big)\Big)\,dr_+, \quad (25)$$

where upper and lower limits r_2 and r_1 should satisfy the following relations

$$T_0 = -\frac{a^2\left(\frac{3(1-b)}{r_2} - 8\pi P r_2\right) - 24\pi P r_2^3 - 9\alpha w r_2^{-3w} - 3(1-b)r_2}{12\pi\left(a^2 + r_2^2\right)}, \quad (26)$$

$$T_0 = -\frac{a^2\left(\frac{3(1-b)}{r_1} - 8\pi P r_1\right) - 24\pi P r_1^3 - 9\alpha w r_1^{-3w} - 3(1-b)r_1}{12\pi\left(a^2 + r_1^2\right)}. \quad (27)$$

Through above equations, one can develop the following results

$$0 = 8\pi P(r_2 - r_1) + 3w\alpha\left(\frac{1}{r_2^{2+3w}} - \frac{1}{r_1^{2+3w}}\right) + (1-b)\left(\frac{1}{r_2} - \frac{1}{r_1}\right) + a^2\left(-\frac{16}{3}\pi P\left(\frac{1}{r_2} - \frac{1}{r_1}\right) - 3\alpha w\left(\frac{1}{r_2^{4+3w}} - \frac{1}{r_1^{4+3w}}\right) - 2(1-b)\left(\frac{1}{r_2^3} - \frac{1}{r_1^3}\right)\right), \quad (28)$$

and

$$8\pi T_0 = +8\pi P(r_2 + r_1) + 3w\alpha\left(\frac{1}{r_2^{2+3w}} + \frac{1}{r_1^{2+3w}}\right) + (1-b)\left(\frac{1}{r_2} + \frac{1}{r_1}\right) + a^2\left(-\frac{16}{3}\pi P\left(\frac{1}{r_2} + \frac{1}{r_1}\right) - 3\alpha w\left(\frac{1}{r_2^{4+3w}} + \frac{1}{r_1^{4+3w}}\right) - 2(1-b)\left(\frac{1}{r_2^3} + \frac{1}{r_1^3}\right)\right). \quad (29)$$

On integrating Eq. (25), we get

$$\pi T_0(r_2^2 - r_1^2) = \frac{(r_2 - r_1)(1-b)}{2} + \frac{4}{3}\pi P\left(\frac{1}{r_2^3} - \frac{1}{r_1^3}\right) - \frac{\alpha}{2}\left(\frac{1}{r_2^{3w}} - \frac{1}{r_1^{3w}}\right) + a^2\left(\frac{(r_1 - r_2)(1-b)}{r_1 r_2} - \frac{8}{3}\pi P(r_2 - r_1) + \frac{3\alpha w}{2(3w+2)}\left(\frac{1}{r_2^{2+3w}} - \frac{1}{r_1^{2+3w}}\right)\right). \quad (30)$$

Putting $y = \frac{r_1}{r_2}$ where y lies in the interval $[0, 1]$, Eqs. (28)–(30) can be re-written as

$$8\pi T_0 = 8\pi P r_2(1+y) + 3w\alpha\left(\frac{1 + y^{2+3w}}{x^{2+3w} r_2^{2+3w}}\right) + \left(\frac{(1+y)(1-b)}{y r_2}\right) - a^2\left(\frac{16\pi P(1+y)}{3 y r_2} + 3\alpha w\left(\frac{1 + y^{4+3w}}{y^{4+3w} r_2^{4+3w}}\right) + 2\left(\frac{(1+y^3)(1-b)}{y^3 r_2^3}\right)\right), \quad (31)$$

$$0 = 8\pi P r_2(1-y) - 3w\alpha\left(\frac{1 - y^{2+3w}}{y^{2+3w} r_2^{2+3w}}\right) - \left(\frac{(1-b)(1-y)}{y r_2}\right) + a^2\left(\frac{16}{3}\pi P\left(\frac{1-y}{y r_2}\right) + 3\alpha w\left(\frac{1 - y^{4+3w}}{y^{4+3w} r_2^{4+3w}}\right) + 2\left(\frac{(1-b)(1-y^3)}{y^3 r_2^3}\right)\right), \quad (32)$$

and

$$\pi T_0 r_2^2(1 - y^2) = \frac{4}{3}\pi P r_2^3(1 - y^3) + \alpha\left(\frac{1 - y^{3w}}{2y^{3w} r_2^{3w}}\right) + \left(\frac{r_2(1-b)(1-y)}{2}\right) + a^2\left(\frac{(y-1)(1-b)}{r_2 y} - \frac{8\pi}{3}P r_2(1-y) - 3\alpha w\left(\frac{1 - y^{2+3w}}{2(2+3w)y^{2+3w} r_2^{2+3w}}\right)\right)\Bigg)\,. \quad (33)$$

Using Eqs. (31) and (33), we get a relation independent of T_0 as

$$\frac{8\pi P r_2(1-y)^2}{3(y+1)} + \alpha r_2^{-3w-2} y^{-3w}\left(\frac{3w\left(y^{3w+2}+1\right)}{y^2} - \frac{4\left(1 - y^{3w}\right)}{1 - y^2}\right) + \frac{\left(\frac{y+1}{y} - \frac{4}{y+1}\right)(1-b)}{r_2} + a^2\left(-\frac{16\pi P(1-y)^2}{3 r_2 y(y+1)} + 3\alpha w r_2^{-3w-4} x^{-3w-2} \times \left(\frac{4\left(1 - y^{3w+2}\right)}{1 - y^2} - \frac{y^{3w+4}+1}{y^2}\right) + \frac{2(1-b)\left(\frac{4}{y+1} - \frac{y^3+1}{x^2}\right)}{r_2^3 y}\right) = 0. \quad (34)$$

Eq. (32) generates the following explicit expression of pressure

$$8\pi(1-y)P = \frac{-1}{3 r_2^6 y^5}\left(a^2\left(3\alpha w r_2^{1-3w} y^{1-3w}\left(-(3y+2)y^{3w+3} + 2y + 3\right) + 2r_2^2 y^2(1-b)\left(-3y^3 - y^2 + y + 3\right)\right)\right) - \frac{(1-y)(1-b)}{r_2^2 y} - 3\alpha w r_2^{-3w-3} y^{-3w-2}\left(1 - y^{3w+2}\right).$$

Putting the above equation in Eq. (34), we reach at

$$b + \frac{1}{3}a^2\left(2(1-b)\left(3y^2 + 13y + 3\right) r_2^{-2} y^{-2} + \frac{3\alpha w r_2^{-3w-3} x^{-3w-3}}{(1-y)^3} \times \left(-2y^{3w+3} + 28y^{3w+4} - 5y^{3w+5} - 3y^{3w+6} + 2y^3 - 28y^2 + 5y + 3\right)\right) - \frac{3\alpha r_2^{-3w-1} y^{-3w-1}}{(1-y)^3}\left(w\left((y+1)\left(1 - y^{3w+3}\right) - 2y^2\left(1 - y^{3w}\right)\right) - 2y^2\left(1 - y^{3w}\right)\right) = 1, \quad (35)$$

which can further be expressed as

$$(1-b)r_2^2 = \sigma(-f_1(y,w)r^2 + a^2 f_2(y,w)) + a^2 f_3(y,b), \quad (36)$$

where

$$f_1(y,w) = \frac{y^{-3w-1}\left(w\left((y+1)\left(1 - y^{3w+3}\right) - 2y^2\left(1 - y^{3w}\right)\right) - 2y^2\left(1 - y^{3w}\right)\right)}{(1-y)^3},$$

$$f_2(y,w) = \frac{w y^{-3w-3}}{3(1-y)^3}(-2y^{3w+3} + 28y^{3w+4} - 5y^{3w+5} - 3y^{3w+6} - 2y^3 - 28y^2 + 5y + 3), \quad f_3(y,b) = \frac{2(1-b)\left(3y^2 + 13y + 3\right)}{3y^2},$$

$$\sigma = -\frac{B_c r_2^{-3w-1} r_c^{3w+1}}{2\pi w}, \quad B_c = -\frac{6w\pi\alpha}{r_c^{3w+1}},$$

here B_c be the unit thickness of BH horizon. It is noticed that $f_5(y,w) = 0$ for $w = -\frac{2}{3}$, and for $a = 0$, the expressions are the same as obtained for charged AdS BH [33].

As $y \to 1$, $r_1 = r_2 = r_c$ (r_c denotes the critical radius of BH horizon), this equality turns Eq. (36) to following form

$$\frac{1-b}{6} = -\frac{B_c}{8\pi}(w+1)(3w+2) + \frac{4\pi a^2}{A_c}\left(\frac{19(1-b)}{9} + \frac{B_c}{54\pi} \times (-50 + w(1 + 6w)(41 + 33w))\right), \quad (37)$$

where $A_c = 4\pi r_c^2$ stands for the critical area of the horizon. For assigned values of a, the value of r_c can be found. Thus from Eq. (37), it can be seen that the position of PT point not only depends on the size of BH but also depends on the parameters a, b, B_c and w. Applying limit $y \to 1$

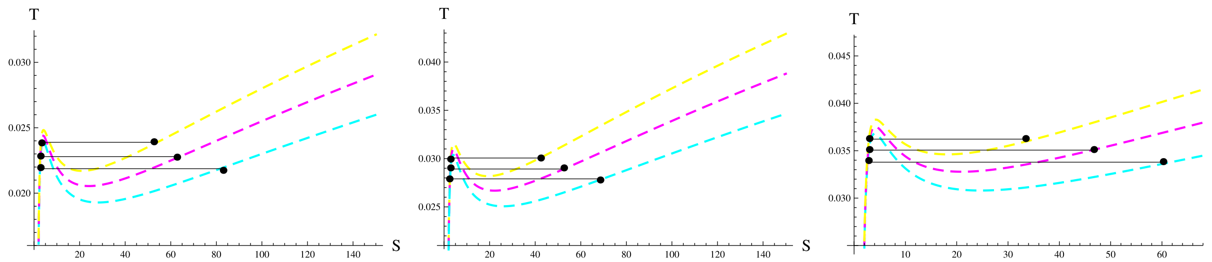

Fig. 3. Temperature versus entropy for $J = 0.1$, $B_c = 0.05$, $w = -\frac{1}{3}$ at constant pressure. The plots from left to right correspond to $b = 0.6, 0.5, 0.4$ and trajectories from top to bottom correspond to $P = 0.9P_c$, $P = 0.8P_c$ and $P = 0.7P_c$, respectively.

Table 1
Numerical values of y, r_2 and T_0 at constant pressure with $B_c = 0.05$, $J = 0.1$ and $w = -\frac{1}{3}$.

b	χ	y	r_2	T_0
0.4	0.7	1.0660	1.4023	0.0348
	0.8	1.0667	1.4118	0.03582
	0.9	1.0674	1.4219	0.03682
0.5	0.7	1.0708	1.3976	0.02868
	0.8	1.0709	1.4066	0.02941
	0.9	1.0710	1.41602	0.03026
0.6	0.7	1.0763	1.3912	0.0225
	0.8	1.0764	1.3993	0.0231
	0.9	1.07648	1.40778	0.02401

on Eq. (34), we can get P_c as

$$P_c = \frac{3}{8\pi}\left(\frac{1-b}{r_c^2} - \frac{B_c(3w+2)(3w+4)r^{3w+1}r_c^{-3w-3}}{6\pi} + 16J^2\left(-\frac{11(1-b)}{r_c^4} - \frac{B_c(3w+4)\left(18w^2+18w-2\right)r^{3w+1}r_c^{-3w-5}}{6\pi}\right)\right), \tag{38}$$

and T_c takes the form as under

$$T_c = \frac{27\alpha w(w+1)^2 r_2^{-3w-2}}{4\pi} + \frac{1-b}{\pi r_2} + 16J^2\left(-\frac{37(1-b)}{4\pi r_2^3} + \frac{\alpha w\left(\frac{81w^3}{2} + 90w^2 + \frac{81w}{2} - \frac{43}{3}\right) r_2^{-3w-4}}{\pi}\right). \tag{39}$$

With the help of previous equations, we can discuss the criticality of thermodynamic variables. It is noticed that this approach is more appropriate as compared to the usual method to calculate the critical values of the complicated BHs.

To get the explicit equation of r_2, Eq. (36) takes the following form

$$r_2^2 = \frac{\frac{J^2}{0.25^2}\left(1 + f_2(y,w)\sigma\right) + f_3(y,b)}{1 - b + f_1(y,w)\sigma}. \tag{40}$$

Inserting the expression of r_2^2 in Eq. (35) and letting that $P_0 = \chi P_c$ where $\chi \in [0,1]$, we get a relation independent of r_2. For assigned values of J, w, B_c and χ, the values of y can be solved numerically. Substituting the derived values of y in Eq. (37), we can find r_2, and r_1 can be obtained from the relation $r_1 = yr_2$. Ultimately, the expression of T_0 can also be obtained (from Eq. (31)). Table 1 illustrates the numerical values of y, r_2 and T_0 for fixed $B_c = 0.05$, $J = 0.1$ and $w = -\frac{1}{3}$. From the following expression

$$T = \frac{1}{8\pi}(16J^2\left(\frac{B_c r_+^{-3w-4} r_c^{3w+1}}{\pi} - \frac{32\pi P\chi}{3r_+} - \frac{4(1-b)}{r_+^3}\right) - \frac{B_c r_+^{-3w-2} r_c^{3w+1}}{\pi} + 16\pi P r_+\chi + \frac{2(1-b)}{r_+}), \tag{41}$$

The $T - S$ trajectories taking relation $P = \chi P_c$ are plotted. To study the effect of b, EoS, and quintessence parameters on the PT point, we draw the trajectories at the constant pressure as represented in Figs. 3–5. The horizontal line of black color in Fig. 3 represents the co-existence space of two phases and the point at which it intersects the curve tells the position of the first-order PT. At a specific pressure P (less than P_c), where $r_+ < r_1$, BH relates to the liquid state, but for $r_+ > r_2$, it shows the vapor phase of the vdW system. When the radius of the BH event horizon belongs to the range $r_1 \leq r_+ \leq r_2$, the BH associates with the vapor–liquid co-existence phase of the vdW system.

It is noticed that the point of PT and the region of the co-existence phase increase with an increment in b at the same pressure (Fig. 3). Thus, the PT in a rotating BH does not depend on its size only but on J and w also, affect its position. It is noted that the temperature of BH decreases for larger values of b. Additionally, the temperature drops down for large values of w and J (Figs. 4, 5). It is observed that isobar in the isobaric decreases with increasing pressure. In the co-existing regions, the BH's evolution is dissimilar from Hawking's phenomena. The BH temperature is higher because of the emission of Hawking radiation but these radiation do not change the temperature and pressure of BH in co-existing regions.

4. Thermal fluctuations

Now we discuss the influence of TF on the stability of KAdS BH surrounded by quintessence and strings cloud. For a system in thermodynamic equilibrium, the statistical properties are described by the partition function which is a function of temperature and some other parameters such as volume. The partition function is the key quantity of the canonical ensemble, from which we can find the Helmholtz free energy, and hence all thermodynamic properties, such as total energy, entropy, and pressure. To calculate the modified entropy against TF, we use the canonical partition function which applies to a canonical ensemble (the system is permitted to exchange heat with the surroundings at fixed volume, temperature, and number of particles). The canonical partition function becomes

$$\mathcal{Z}(\delta) = \int_0^\infty \exp(-\delta E)\sigma(E)dE, \tag{42}$$

with $T = \frac{1}{\delta}$, and E be the average energy of the system and $\sigma(E)$ represents its quantum density. Implementing inverse Laplace transformation, the states density is computed as

$$\sigma(E) = \frac{1}{2\pi i}\int_{c-i\infty}^{c+i\infty} \exp(\delta E)\mathcal{Z}(\delta)d\delta = \frac{1}{2\pi i}\int_{c-i\infty}^{c+i\infty} \exp(S_0(\delta))d\delta, \tag{43}$$

here $S_0 = \ln \mathcal{Z} + \delta E$ be the corrected entropy and c is a positive constant. Via steepest descent method about saddle point δ, the above mentioned integral turn out to be

$$S_0(\delta) = S + \frac{1}{2}(\delta - c)^2 \frac{d^2 S}{d\delta^2}|_{\delta=c} + \text{higher-order terms}, \tag{44}$$

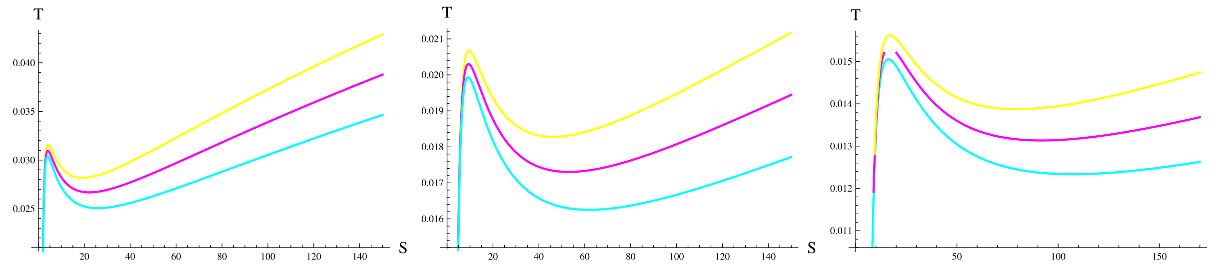

Fig. 4. Temperature versus entropy for $b = 0.5$, $B_c = 0.05$, $w = \frac{-1}{3}$ at constant pressure. The plots from left to right correspond to $J = 0.1, 0.15, 0.2$, respectively.

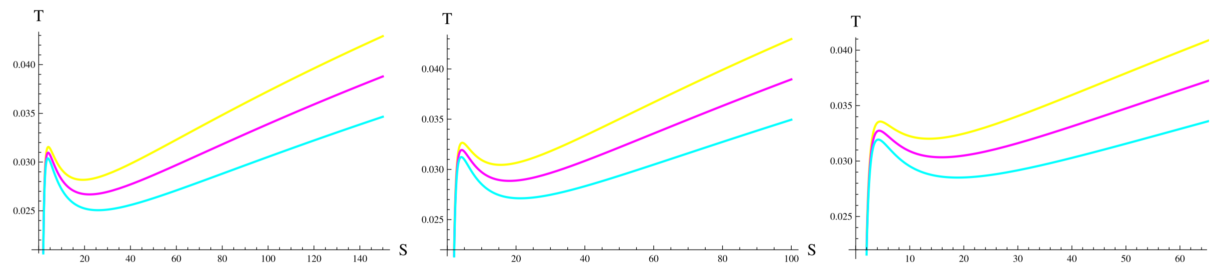

Fig. 5. Temperature versus entropy for $b = 0.5$, $B_c = 0.05$, $J = 0.1$ at constant pressure. The plots from left to right correspond to $w = -\frac{1}{3}, -\frac{1}{2}, -\frac{3}{4}$, respectively.

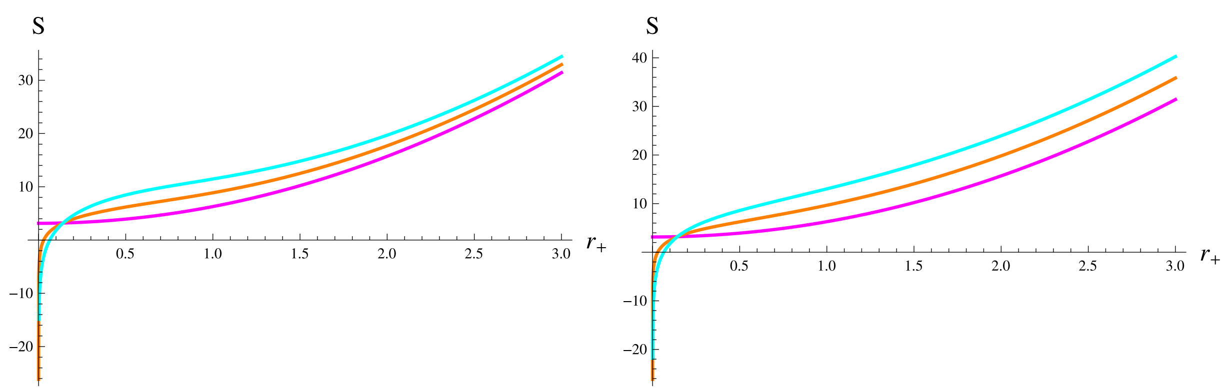

Fig. 6. S versus r_+ for $a = 1$, $\alpha = 1.5, b = 0.5$ with $w = -\frac{1}{2}$ (left panel) and $w = -\frac{7}{10}$ (right panel). Here $\delta = 0$, 0.5 and 1 are elaborated by magenta, orange and cyan colors, respectively.

where $S = S_0(\delta)$ be the zeroth order entropy along with vanishing $\frac{\partial S}{\partial \delta}$ and $\frac{\partial^2 S}{\partial \delta^2} > 0$ at the point $\delta = c$. Using Eqs. (43) and (44), we obtain

$$\sigma(E) = \frac{e^S}{2\pi i} \int_{c-i\infty}^{c+i\infty} \exp\left(\frac{1}{2}(\delta - c)^2 \frac{d^2 S_0}{d\delta^2}\right) d\delta. \quad (45)$$

The density of states function describes the energy distribution of allowed states in the quantum well. Whether or not particular states are occupied by electrons is determined by the electron concentration and the temperature through the thermodynamic properties of the system. It plays an important role in determining the transition rates. After subsequent simplifications, we get density of states as

$$\sigma(E) = \frac{e^S}{\sqrt{2\pi \frac{d^2 S_0}{d\delta^2}}}, \quad (46)$$

which gives

$$S_0 = S - \delta \ln(ST^2) + \frac{\delta_1}{S},$$

with correction parameters δ and δ_1.

- For $\delta, \delta_1 \to 0$, the original entropy of BH can be restored.
- For $\delta \to 1, \delta_1 \to 0$, the usual logarithmic corrected entropy can be recovered.
- For $\delta \to 0, \delta_1 \to 1$, the second order correction term can be attained, which is varying inversely to original BH entropy.
- For $\delta, \delta_1 \to 1$, the effects of higher-order correction terms can be observed.

In current paper, we worked out for the second case ($\delta \to 1, \delta_1 \to 0$). In the above equation, the second logarithmic term appears because of small fluctuations around the equilibrium position. Since BH is considered a macroscopic stellar object, and TF are effective on microscopic (Planck) scale, therefore the correction terms in logarithmic form have a small contribution in the entropy. Putting Eqs. (8) and (9) in the above equation, the corrected entropy has the following form

$$S_0 = \frac{\pi\left(a^2 + r^2\right)}{1 - \frac{a^2}{l^2}} - \delta \ln\left(\frac{\left(\frac{3r^2\left(\frac{a^2}{3} + r^2\right)}{l^2} - a^2 + (1-b)r^2 + 3\alpha w r^{1-3w}\right)^2}{16\pi r^2\left(1 - \frac{a^2}{l^2}\right)\left(a^2 + r^2\right)}\right), \quad (47)$$

We plot corrected and uncorrected entropy for various parametric values w, b and a, so that the effect of correction terms can be observed. Figs. 6–8 show that uncorrected entropy for $\delta = 0$ exhibiting positive and monotonically increasing behavior, hence fulfills the second law

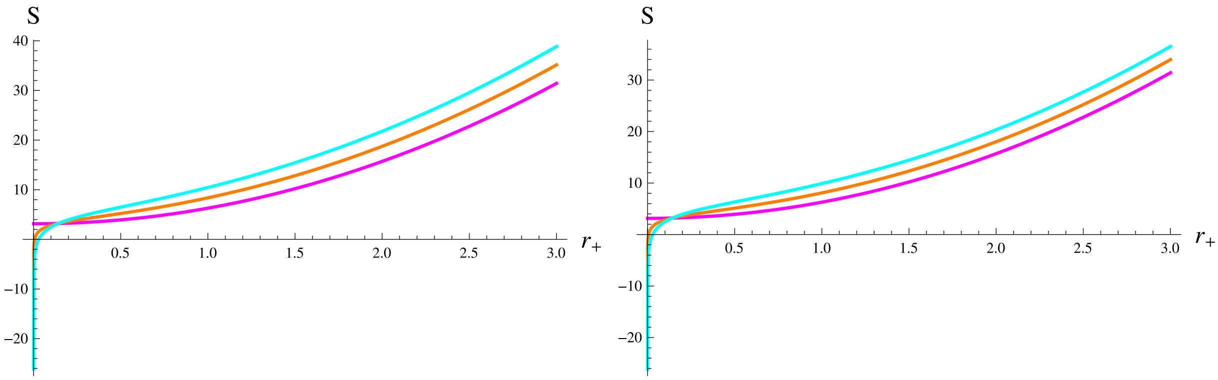

Fig. 7. S versus r_+ for $a = 1 = \alpha$, $w = -\frac{1}{4}$. Left plot: $b = \frac{1}{2}$; Right plot: $b = \frac{9}{10}$.

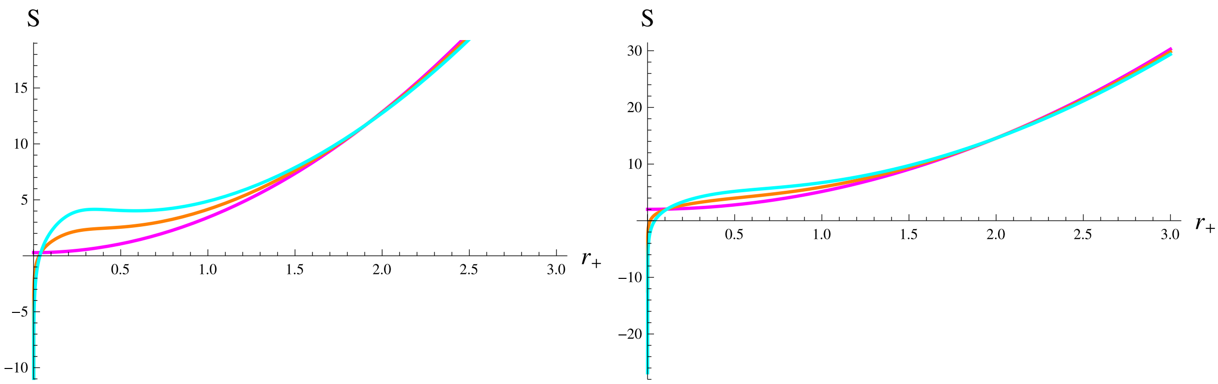

Fig. 8. S versus r_+ taking $b = 0.5$, $\alpha = 2$ and $w = -\frac{2}{3}$. Left plot: $a = \frac{3}{10}$; Right plot: $a = \frac{8}{10}$.

of BH thermodynamics. Under TF, the entropy of small BHs attains negative values for larger values of the correction parameter. It is observed that BH achieves more entropy for smaller values of EoS parameter and b, implying an increment in the BH area. Whereas, the rotation parameter shows the inverse scenario, i.e., the larger values of rotation parameter yield an increment in entropy. It is being observed that for enlarged radius, the corrected and uncorrected entropies follow the same trend, which is in agreement with the fact that TF have no influence on the thermodynamics of large BH.

The first-order corrected HFE ($F = M - TS_0 - PV$) as the Legendre transformation of the internal energy is given by

$$F = -\frac{\frac{3r^2\left(\frac{a^2}{3}+r^2\right)}{l^2} - a^2 + (1-b)r^2 + 3\alpha w r^{1-3w}}{4\pi r\left(a^2+r^2\right)} \times \frac{\frac{\pi(a^2+r^2)}{1-\frac{a^2}{l^2}} - \delta \ln\left(\frac{\left(\frac{3r^2\left(\frac{a^2}{3}+r^2\right)}{l^2} - a^2 + (1-b)r^2 + 3\alpha w r^{1-3w}\right)^2}{16\pi r^2\left(1-\frac{a^2}{l^2}\right)(a^2+r^2)}\right)}{4\pi r\left(a^2+r^2\right)} + \frac{\frac{r^2(a^2+r^2)}{l^2} + a^2 + (1-b)r^2 - \alpha r^{1-3w}}{2r\left(1-\frac{a^2}{l^2}\right)^2} + \frac{\left(a^2+r^2\right)\left(a^2l^2 - a^2r^2 + 2l^2r^2\right)}{4l^4 r\left(1-\frac{a^2}{l^2}\right)^2} - \frac{a^2bl^2r^2 - \frac{2a^2bl^2r^2(l^2+r^2)}{a^2+r^2} - a^2\alpha l^2 r^{1-3w}}{4l^4 r\left(1-\frac{a^2}{l^2}\right)^2}.$$

Fig. 9 represents that for $-\frac{2}{3} < w \leq -\frac{1}{3}$, the free energy F gains positive values for the BH of small size, and shows opposite trend for large BH (left plot). Whereas, for $-1 < w \leq -\frac{2}{3}$, it attains positive values all over the domain (right panel of Fig. 9). It can be seen that the correction parameter increases/decreases the HFE before/after r_c, respectively. The effect of string cloud parameter b, on the free energy F is checked in Fig. 10. It 10 shows that F remains positive for the BH of small size, and remains negative for large size BH. The value of F increases with the increase of parameter b.

The corresponding GFE ($G = M - TS_0$) is calculated in the following form

$$G = \frac{1}{4r_+}\Bigg(\Big(r_+^{-3w}\left(r_+^{3w}\left(l^2a^2 - r_+^2\left(a^2+l^2\right) - 3r_+^4\right) - 3\alpha l^2 r_+ w\right) \times \Big(\ln\left(\frac{r_+^{-6w-2}\left(r_+^{3w}\left(l^2a^2 - r_+^2\left(a^2+l^2\right) - 3r_+^4\right) - 3\alpha l^2 r_+ w\right)^2}{16\pi l^2\left(l^2-a^2\right)\left(a^2+r_+^2\right)}\right) \times \delta(a^2-l^2) + \pi l^2\left(a^2+r_+^2\right)\Big)\Big)\left(\pi l^2\left(l^2-a^2\right)\left(a^2+r_+^2\right)\right)^{-1} + \frac{2\left(\frac{r_+^2\left(a^2+r_+^2\right)}{l^2} + a^2 - \alpha r_+^{1-3w} + r_+^2\right)}{\left(\frac{a^2}{l^2}-1\right)^2}\Bigg). \tag{48}$$

Figs. 11 and 12 indicate that GFE exhibit the same trend as that of HFE. It is known that $G > 0$ related to unnatural reactions (which needs an exterior energy source) whereas $G < 0$ represents natural reactions (which do not need any exterior source). Black holes with $G < 0$ are stable thermodynamically as they radiate their energy in the exterior region to attain the low energy state. From Fig. 11 (left and right plots), it is clear that large BHs are thermodynamically stable for $-\frac{2}{3} < w \leq -\frac{1}{3}$ as compared to small BHs as $G > 0$ initially. For $-1 < w \leq -\frac{2}{3}$, the uncorrected system remains unstable while the BH under fluctuations effects gradually moves towards stability. This is resulted that larger values of EoS parameters produce more stable model. Fig. 12 depicts

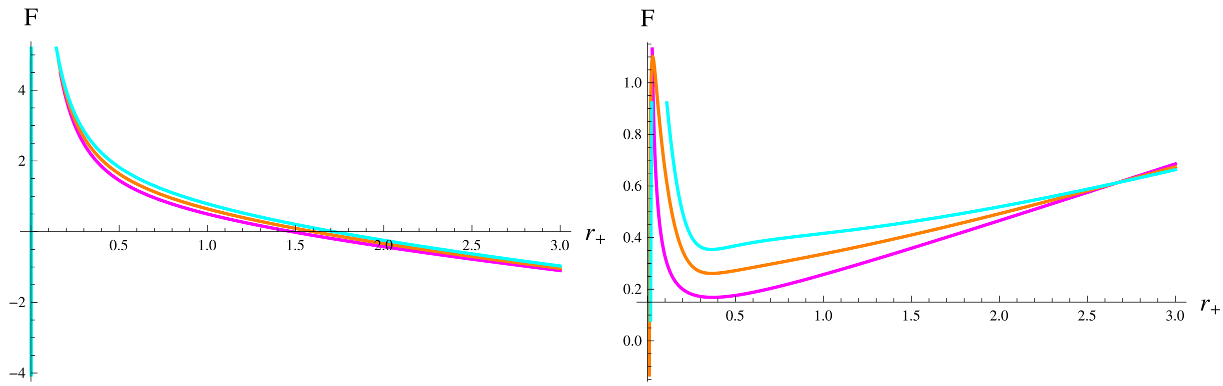

Fig. 9. HFE versus r_+ for $b = 1 = a$, $\alpha = 2$ and $w = -\frac{1}{3}$ (left panel); $w = -\frac{2}{3}$ (right panel).

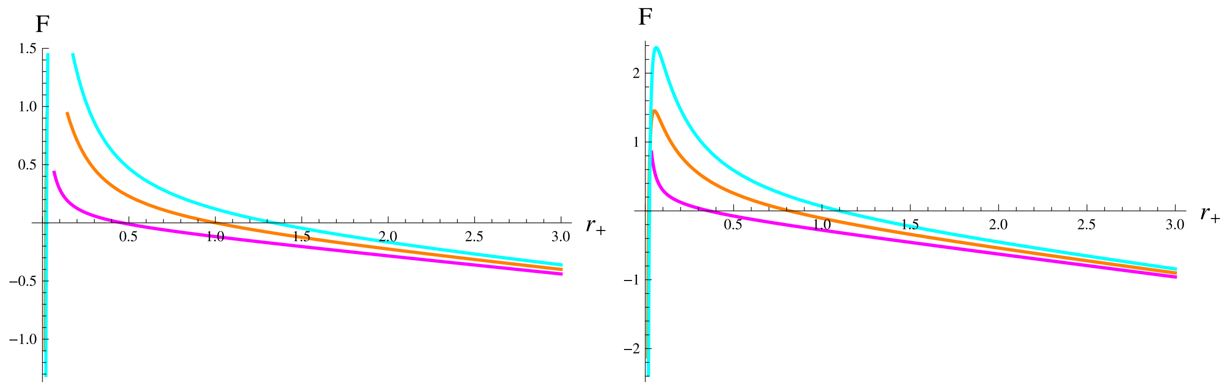

Fig. 10. HFE versus r_+ for $w = -\frac{1}{3}$, $\alpha = 1.5$ and $a = 0.2$. Left panel: $b = \frac{1}{10}$. Right panel: $b = \frac{4}{5}$.

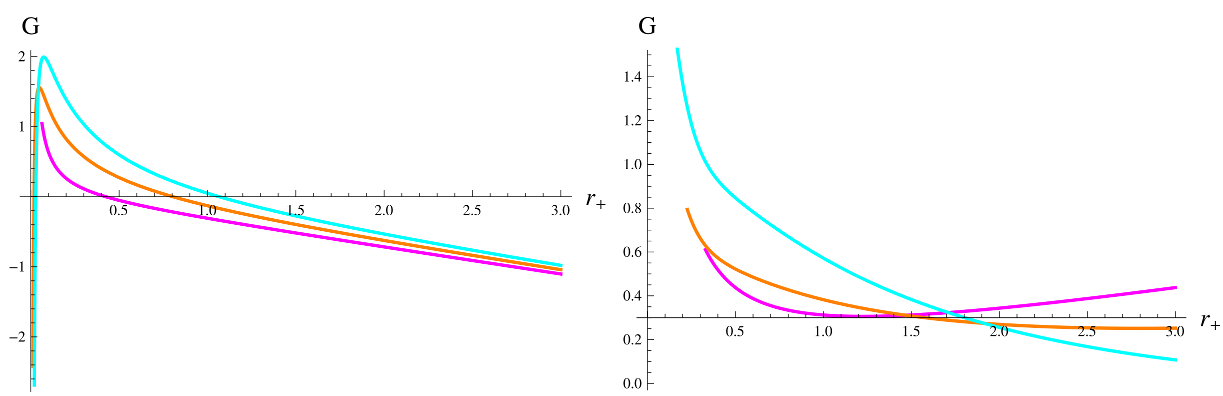

Fig. 11. GFE versus r_+ for $b = \frac{1}{2}, a = \frac{3}{10}$, $\alpha = 2$ and $w = -\frac{1}{3}$ (left panel); $w = -\frac{2}{3}$ (right panel).

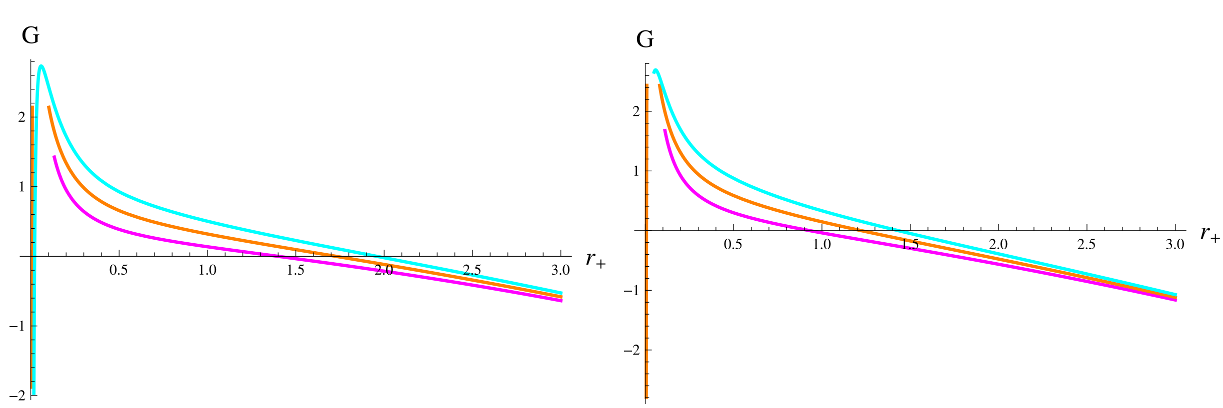

Fig. 12. GFE versus r_+ for $a = \frac{1}{2} = -w$, $\alpha = 2$ and $b = 0.2$ (left panel); $b = 0.9$ (right panel).

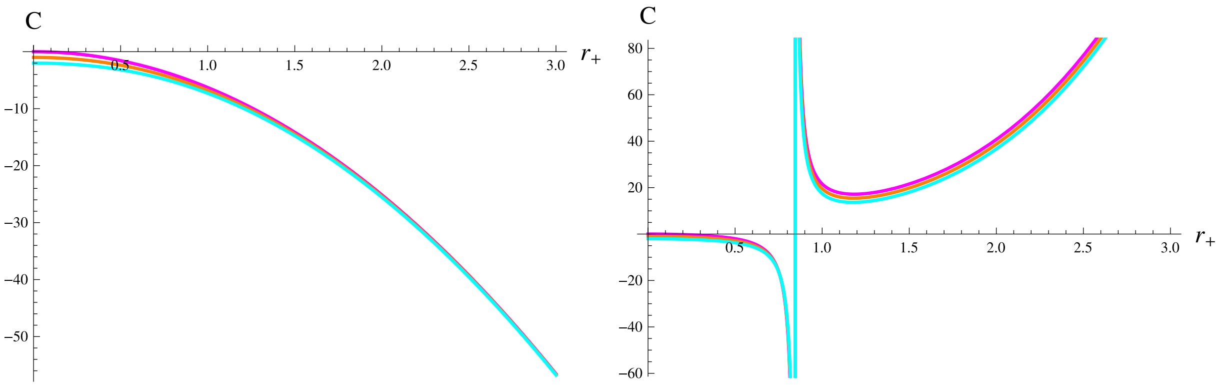

Fig. 13. C versus r_+ for $a = 1$, $\alpha = 1 = b$ with $w = -\frac{2}{3}$ (left panel) and $w = -\frac{1}{3}$ (right panel).

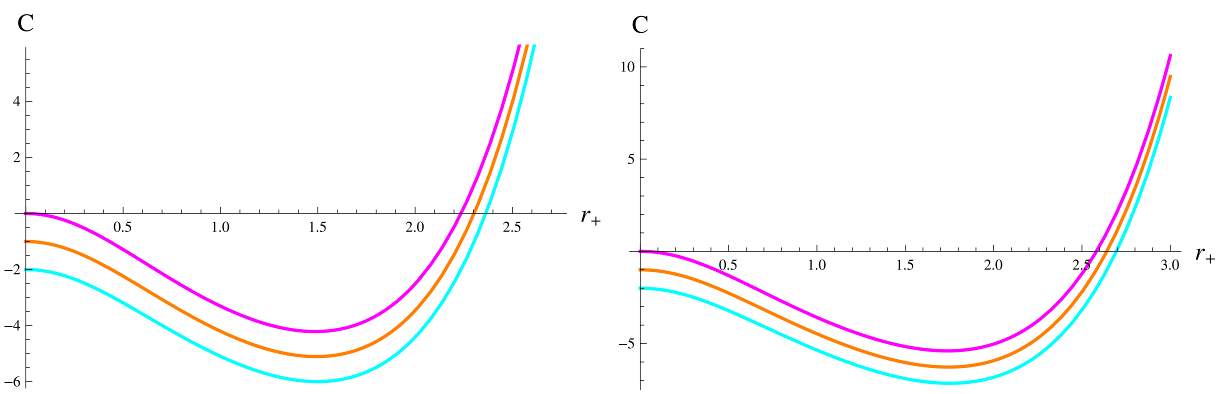

Fig. 14. C versus r_+ for $w = -\frac{1}{3}$, $\alpha = 0.1$ and $a = 2$ with $b = 0.3$ (left panel) $b = 0.1$ (right panel).

the effect of strings cloud parameter, $G > 0$ initially then goes to negative values for the BH of large size for increasing values of b. The model is thermodynamically stable for increasing values of string cloud parameter.

For the considered model, the specific heat (C) is calculated as

$$\begin{aligned} C = T\frac{\partial S_0}{\partial T} &= 2\left(-a^6\delta\left(l^2+r^2\right)r^{3w} + a^4\left(-l^2\left(\delta\left(-(b-2)r^{3w+2} - 9\alpha r w^2\right)\right.\right.\right. \\ &\left. +\pi r^{3w+4}\right) + l^4\left(\delta+\pi r^2\right)r^{3w} - 9\delta r^{3w+4}\Big) + a^2\Big(l^4\Big(\delta\Big(-(b-3)r^{3w+2} \\ &-9\alpha r w^2\Big) + \pi r^2\left(b r^{3w+2} - 3\alpha r w\right)\Big) - l^2 r^2\Big(\delta\left(-3r\left(3r^{3w+1} + \alpha w(3w+1)\right)\right) \\ &+4\pi r^{3w+4}\Big) - 6\delta r^{3w+6}\Big) + l^2 r^2\Big(l^2\Big(\pi r^2\left((b-1)r^{3w+2} - 3\alpha r w\right) \\ &+\delta\left(-3\alpha r w(3w+1)\right)\Big) - 3\left(\pi r^2 - 2\delta\right)r^{3w+4}\Big)\Big) \times \\ &\Big\{\left(a^2-l^2\right)\Big(a^4\left(l^2+r^2\right)r^{3w} + a^2\Big(l^2\left(-(b-4)r^{3w+2} - 9\alpha r w^2\right) \\ &+8r^{3w+4}\Big) + r^2\Big(l^2\left(r\left((b-1)r^{3w+1} - 3\alpha w(3w+2)\right)\right) \\ &+3r^{3w+4}\Big)\Big)\Big\}^{-1}. \end{aligned}$$

The divergence points of C are called the PT points, and its signature tells us about thermal stability of a BH. The region $C > 0$ ensures thermal stable phase while $C < 0$ represents the instable region. The specific heat is being plotted in Figs. 13 and 14 for our considered model. The left plot of Fig. 13 indicates that the specific heat remains negative throughout r_+ for $w = -\frac{2}{3}$, so model is unstable at this value. Also, we observe that the TF do not affect the position of PT. In right plot, one can see that large BHs are stable thermally as value of C lies is positive whereas BHs with small radius get negative heat capacity, due to which the system becomes unstable. Generally, we found that the model remained unstable ($C < 0$) for $-1 < w < -\frac{5}{3}$ and stable ($C > 0$) for $-\frac{5}{3} < w < -\frac{1}{3}$. Fig. 14 (left and right plot) shows that the model is shifting instability to stability for increasing values of the cloud of strings parameter. It is clear from Fig. 14 that larger values of b produce more negative range of C for small BH without disturbing the large BH geometries. It is interesting to note that for the larger values of b, the system becomes stable at small horizon radius as compared to its smaller values. In general, the model remains stable when string cloud parameter lies in the range $0 < b \leq 0.85$. This illustrates that TF influence the stability of BHs with small radius while the large radius BHs mostly remain unaffected.

5. Conclusions

In theoretical physics, the discussion about the $P-V$ criticality and thermal properties of BHs has always been a captivating scenario. In this paper, we have analyzed the combined effects of QDE and cloud of strings on rotating KAdS BH. To this end, we have computed the expression of thermodynamical variables including Hawking temperature, entropy, angular momentum, and volume of the BH. In EPS, these thermodynamic variables hold the SGD relation in the appearance of both quintessence and cloud of the string parameter. The graphical analysis of temperature versus entropy shows that temperature is sensitive for all the involved model parameters and decreases with the increase of rotation and strings cloud parameters. Whereas the EoS parameter affects the BH's temperature slightly. We have calculated the critical expressions of temperature and pressure in two different ways that are vdW-type EoS and MEAL. The latter technique is found to be more reasonable to examine the criticality of the complex BHs. Using MEAL, we plot a PS diagram in $T-S$ conjugate variables and obtain an isobar, which represents the co-existence region of liquid–gas phases. Moreover, we have computed the corrected entropy to inspect the influence of TF on the stability of KAdS BH.

It is well-known that BH associates with the vapor–liquid co-existence phase if isobaric contains an area where the state of stable equilibrium is not fulfilled. Like the vdW framework, the non-physical oscillating area is replaced with an isobar represented by the solid horizontal line of black color which depicts the co-existence space of two phases. Using MEAL, we have drawn the trajectories in $T-S$ plane to find the location of isobar at different pressures. It is noticed that the point of PT and the region of the co-existence phase increases with an increment in b at the same pressure (Fig. 3). Thus, the PT in a rotating BH did not depend on its size only but J and w affect its position also. It is noted that the temperature of BH decreases for larger values of b. Additionally, the temperature drops down for large values of w and J (Figs. 4, 5). It is observed that isobar in the isobaric decreases with increasing pressure.

Finally, we have discussed the influence of TF on the stability of KAdS BH through trajectories of corrected and uncorrected entropy for different values of b and w and a. It is observed that BH achieves more entropy for smaller values of the EoS parameter and b, implying an increment in the BH area. Whereas, the rotation parameter shows the inverse scenario, i.e., the larger values of the rotation parameter yield an increment in entropy. It is being observed that for enlarged radius, the corrected and uncorrected entropies follow the same trend, which agrees with the fact that TF has no influence on the thermodynamics of BHs with larger radii [45]. It is resulted that model is thermodynamically stable for increasing values of string cloud parameter as GFE becomes negative for small critical radius. Moreover, larger values of EoS parameters produce a more stable model as large BHs are thermodynamically stable for $-\frac{5}{3} < w \leq -\frac{1}{3}$ as compared to small BHs which is consistent with literature [34]. It is also found that b should lie in the interval $[0, 0.85]$ to attain a stable model.

We have also analyzed the local stability of considered gravitational geometry through specific heat and found similar results as obtained in Gibbs energy. It is concluded that BH experiences first-order phase transition and its position remain unchanged under logarithmic corrections. Thus, TF have much influence on BHs with a small horizon radius while large BHs mostly remain unaffected. It is worthy to mention here that for $b = 0$, all derived results reduced to quintessential rotating AdS BH [34].

For future directions, we can discuss the phase transition and thermodynamical behavior of Bardeen–Kiselev AdS BH.

Declaration of competing interest

The authors declare that they have no known competing financial interests or personal relationships that could have appeared to influence the work reported in this paper.

Data availability

Data will be made available on request.

References

[1] P.S. Letelier, Phys. Rev. D 20 (1979) 1294.
[2] M. Barriola, A. Vilenkin, Phys. Rev. Lett. 63 (1989) 341.
[3] C. Bernard, Phys. Rev. D 94 (2016) 085007.
[4] G. Tokgöz, I. Sakalli, Classical Quantum Gravity 34 (2017) 125007.
[5] A. Al-Badawi, I. Sakalli, S. Kanzi, Ann. Physics 412 (2020) 168026.
[6] G. Tokgöz, I. Sakalli, Int. J. Geom. Methods Mod. Phys. 17 (2020) 2050143.
[7] J. Sadeghi, S.N. Gashti, E.N. Mezerji, B. Pourhassan, arXiv:2011.05109.
[8] A. Al-Badawi, Gen. Relativ. Gravi. 54 (2022) 1.
[9] I. Sakalli, S. Kanzi, Turk. J. Phys. 46 (2022) 51.
[10] S. Perlmutter, et al., Astrophys. J. 517 (1999) 565.
[11] V.V. Kiselev, Classical Quantum Gravity 20 (2003) 1187.
[12] S. Chen, B. Wang, R. Su, Phys. Rev. D 77 (2008) 124011.
[13] J.D. Bekenstein, Lett. Nuovo Cimento 4 (1972) 737.
[14] J.D. Bekenstein, Phys. Rev. D 7 (1973) 2333.
[15] S.W. Hawking, Nature 248 (1974) 30.
[16] S.W. Hawking, Comm. Math. Phys. 43 (1975) 199.
[17] S.W. Hawking, Phys. Rev. D 13 (1976) 191.
[18] O. Aharony, S.S. Gubser, J.M. Maldacena, H. Ooguri, Y. Oz, Phys. Rep. 323 (2000) 183.
[19] S.W. Wei, Y.X. Liu, Phys. Rev. D 87 (2013) 044014.
[20] J.L. Zhang, R.G. Cai, H. Yu, J. High Energy Phys. 1502 (2015) 143.
[21] M.B.J. Poshteh, B. Mirza, Z. Sherkatghanad, Phys. Rev. D 88 (2013) 024005.
[22] R.G. Cai, et al., J. High Energy Phys. 09 (2013) 005.
[23] Y.G. Miao, Z.M. Xu, Eur. Phys. J. C 77 (2017) 403.
[24] S. Gunasekaran, D. Kubiznak, R.B. Mann, J. High Energy Phys. 11 (2012) 110.
[25] P. Cheng, S.W. Wei, Y.X. Liu, Phys. Rev. D 94 (2016) 024025.
[26] J. Sadeghi, A.S. Kubeka, Internat. J. Theoret. Phys. 55 (2016) 2455.
[27] J.P.M. Graça, I.P. Lobo, V.B. Bezerra, H. Moradpour, Eur. Phys. J. C 78 (2018) 823.
[28] M.S. Ali, S.G. Ghosh, arXiv:1906.11284.
[29] D.V. Singh, S. Siwach, arXiv:2003.11754.
[30] S.W. Wei, Y.X. Liu, Phys. Rev. D 101 (2020) 104018.
[31] G.Q. Li, Phys. Lett. B 735 (2014) 256.
[32] K.h. Jafarzade, J. Sadeghi, arXiv:1803.04250.
[33] X.Y. Guo, et al., Eur. Phys. J. C 80 (2020) 168.
[34] M. Sharif, Q. Ama-Tul-Mughani, Phys. Dark Universe 30 (2020) 100723.
[35] M. Sharif, Q. Ama-Tul-Mughani, Eur. Phys. J. Plus 136 (2021) 284.
[36] G.Q. Li, Phys. Lett. B 735 (2014) 256.
[37] M. Chabab, S. Iraoui, Gen. Relativ. Gravit. 52 (2020) 75.
[38] G. Gour, A.J.M. Medved, Classical Quantum Gravity 20 (2003) 3307;
F.J. Wang, Y.X. Gui, C.R. Ma, Phys. Lett. B 660 (2008) 144.
[39] B. Pourhassan, M. Faizal, U. Debnath, Eur. Phys. J. C 76 (2016) 145;
B. Pourhassan, K. Kokabi, S. Rangyan, Gen. Relativity Gravitation 49 (2017) 144;
B. Pourhassan, K. Kokabi, Z. Sabery, Ann. Physics 399 (2018) 181.
[40] A. Haldar, R. Biswas, Gen. Relativity Gravitation 50 (2018) 69; Astrophys. Space Sci. 363 (2018) 27.
[41] S. Upadhyay, Gen. Relativity Gravitation 50 (2018) 128.
[42] A.K. Sinha, arxiv:1608.08359; Upadhyay, S. et al.: Prog. Theor. Exp. Phys. 2018 (2018) 093E01.
[43] M. Zhang, Nuclear Phys. B 935 (2018) 170.
[44] M. Sharif, Z. Akhtar, Phys. Dark Universe 29 (2020) 100589.
[45] M. Sharif, Q. Ama-Tul-Mughani, Ann. Physics 422 (2020) 168312; Commun. Theor. Phys. 73 (2021) 085402.
Q. Ama-Tul-Mughani, W. Salam, R. Saleem, Astropart. Phys. 132 (2021) 102623;
Q. Ama-Tul-Mughani, A. Waseem, W.U. Salam, A. Jawad, Chinese J. Phys. http://dx.doi.org/10.1016/j.cjph.2021.11.024.
[46] Z. Xu, J. Wang, Phys. Rev. D 95 (2017) 064015.
[47] M.M. Caldarelli, G. Cognola, D. Klemm, Classical Quantum Gravity 17 (2000) 399.